

Delayed growth of dry area with CHF enhancement on oxidized Cr-nanostructured surfaces

Namgook Kim ^a, Hong Hyun Son ^a, Sung Joong Kim ^{a, b*}

^aHanyang University, 222 Wangsimri-ro, Seongdong-gu, Seoul 04763, Republic of Korea

^bInstitute of Nano Science & Technology, Hanyang University

*Corresponding author: sungkim@hanyang.ac.kr

1. Introduction

Critical heat flux (CHF) is important in terms of the nuclear reactor safety and the efficiency of boiling heat transfer. This parameter is known to enhance with a capillary wicking potential affected by a surface roughness on a material in contact with boiling fluid [1]. In this regard, numerous researchers have tried to quantify the wicking characteristics. However, almost these studies were conducted on the surfaces with micropillar array, porous medium, or excessive roughness, not included in the application for nuclear fuel cladding. In addition, such quantification methods were quite different with the in-situ boiling situation, in which the nucleate bubble grow with the vapor recoil pressure. Thus the objective of this study is to investigate the wicking characterizations of nanostructured metal surfaces by quantifying the growth of dry area to simulate the in-situ boiling. Furthermore, CHF changes were evaluated along with quantified wicking potentials.

2. Experiment

2.1 Sample preparation

In this paper, we selected chromium (Cr) as a target material for a coating. It was deposited on base material by using DC magnetron sputtering following the sputtering conditions as listed in Table I. In particular, we adopted the various substrate temperatures of 150, 300, and 600 °C, which could change the nanoscale roughness. In addition, an oxidation process to Cr-coated surfaces was conducted at ambient temperature of 400 °C for 20 days to variate the nanoscale roughness on surfaces.

Table I: Sputtering condition

Sputtering parameters	Sputtering condition
Target material	Cr
Power (W)	150~160
Gas pressure (torr.)	1.0×10^{-2}
Substrate temperature (°C)	150 / 300 / 600

All the test surfaces used in this study are noted with two terms such as *OxCr-T600*. The first term, *OxCr*, refers to ‘oxidized and Cr-sputtered’. It could be changed with *B* and *Cr*, which refer ‘bare’ and ‘Cr-sputtered’, respectively. The second term, *T600*, refers to ‘sputtered at substrate temperature of 600 °C’. Thus *OxCr-T600* refers to the oxidized test surface sputtered at the substrate temperature of 600 °C.

2.2 Sample characterization

Fig. 1(a) and (b) show the surface morphology of the fresh and oxidized Cr-coated surfaces using NOVA NANO SEM 450, respectively. On the top of this, there were the dome-shaped structures in nanoscale, which were smaller following the substrate temperature and identified as Cr through SEM/EDS. In addition, we could confirm the Cr-coated layer thickness of approximately 1.7 μm with no significant deflection of fine columnar grains by the cross-sectional SEM images as shown in Fig. 1(c). After oxidation process, the oxide layer of Cr was formed above the existing Cr layer in the thickness of approximately 200 nm (the thin and dark line in Fig. 1(c)). The formation of oxide layer modified the existing nanoscale structures to more circular shape with larger size.

It is widely accepted that Cr-sputtering process makes the test surfaces superhydrophilic. We confirmed this here through static contact angle (CA) measurement as shown in the inset images of Fig. 1(a) and (b). CAs of each fabricated samples were approximately 0°

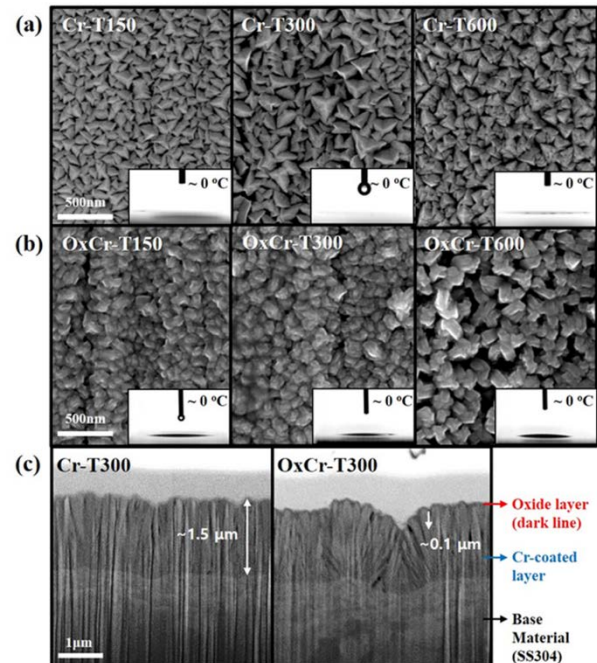


Fig. 1. SEM images of surface morphology on (a) fresh and (b) oxidized Cr-coated surfaces (inset images: static contact angle) and (c) a cross-sectional SEM images of Cr-T300 and OxCr-T300.

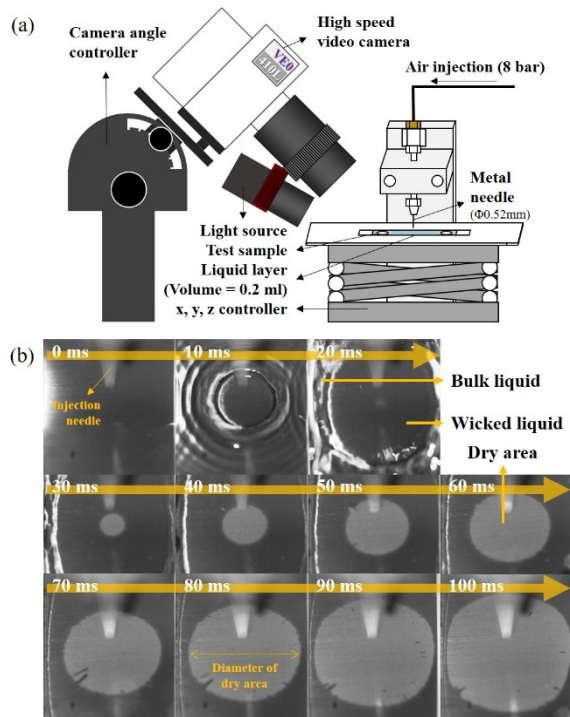


Fig. 2. (a) Schematic diagram of growing dry area measurement instrument; (b) growing behavior of dry area on Cr-T300.

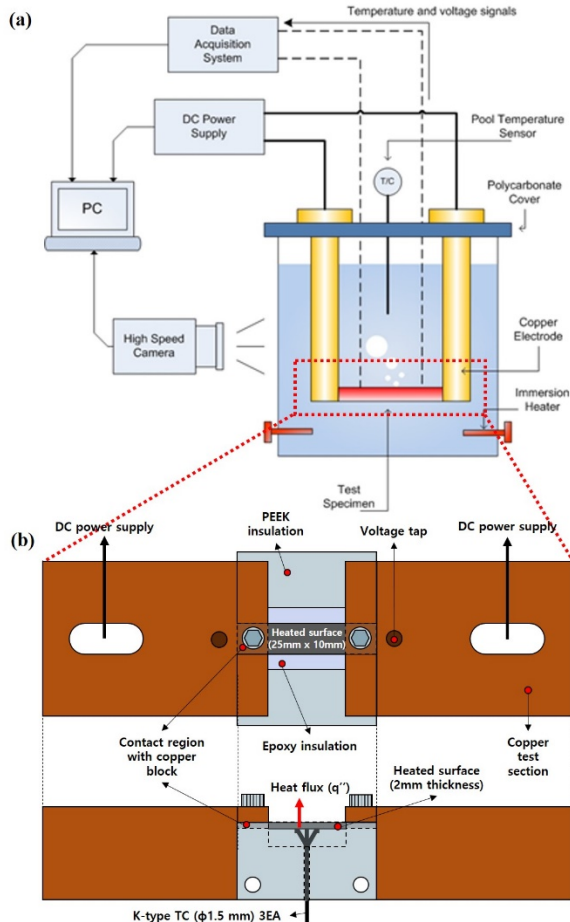


Fig. 3. Schematic diagram of (a) pool boiling apparatus; (b) upper and lateral side test section.

2.3 Experimental setup: visualization of growing dry area caused by a compressed air injection

As mentioned above, it is well known that the superhydrophilicity and resultant CHF enhancement of nanoscale structure comes from the capillary wicking. The capillary wicking characterization of the fabricated surfaces, therefore, need to be analyzed. In addition, this measurement should simulate the in-situ boiling situation. Son et al. [2] found the novel method to characterize the wicking capability with the receding behavior of wicked liquid around expanding dry area by injecting the compressed air. They revealed that the resultant size of dry area has a good linearity with the trend of CHF enhancement and thereby this receding behavior is highly similar with the growth of dry area against the wicked liquid inflow under the nucleate bubble.

Following this, we conducted a similar air injection experiment by using receding behavior measurement instrument as shown in a schematic diagram of Fig. 2(a). The pressure of air compressor was set to 0.8 MPa, of which value belongs to the range of nucleation pressure based on Young-Laplace equation. We visualized the growing behavior of the dry area using a high speed video (HSV) camera with the frame rate of 2,000 fps as shown in Fig. 2(b). After bulk liquid spreading out, a wicked liquid region was exhibited and a dry area slowly expanded on superhydrophilic surface. This behavior was contrast with the bare surface showing the rapidly spreading out due to the absence of wicked region.

2.4 Experimental setup: pool boiling test

Fig. 3 shows a schematic of the pool boiling apparatus and a design of the test section. The length, width, and thickness of the test sample were 45, 10, and 2 mm, respectively. Heat transfer area was $25 \text{ mm} \times 10 \text{ mm} = 250 \text{ mm}^2$. Polyether ether ketone (PEEK) and epoxy were used for thermal and electrical insulations. Temperature and voltage drop were measured with three K-type thermocouples attached underneath the samples and voltage taps attached to the PEEK screw, respectively (Fig. 3(b)).

Direct Joule heating method was used to carefully supply steady state heat flux. Applied heat flux was calculated as following equation.

$$q'' = \frac{\text{Power}}{A_{\text{heated}}} = \frac{VI}{WL_{\text{heated}}} \quad (1)$$

Here, V , I , W , and L_{heated} are the measured voltage drop across the test material, the measured current, the width of the heat transfer area, and the heated length, respectively. Uncertainty of the measured heat flux was estimated as 5.2% based on the error propagation method.

3. Results and discussions

CHF enhancement on each superhydrophilic surfaces was analyzed by conducting the pool boiling experiment. CHF was determined as the heat flux at the time of temperature jump. The measured CHF on the fresh and oxidized Cr-coated surfaces are listed in Table II. The CHF enhancement of Cr-T150/300/600 and OxCr-T150/300/600 was 1.32, 1.25, 1.09, 1.50, 1.37, and 1.30 than bare surface, respectively. Moreover, the CHF on oxidized Cr-coated surfaces was more enhanced than fresh Cr-coated surfaces and the decreasing trend following substrate temperature maintained before and after oxidation process.

Table II: CHF results

Samples	CHF (kW/m ²)	Roughness parameters	
		R _a (nm)	r _n (-)
Bare	713.5	105.3	1.00
Cr-T150	944.1	87.6	1.15
Cr-T300	896.0	92.8	1.13
Cr-T600	778.3	93.8	1.10
OxCr-T150	1056.2	99.4	1.20
OxCr-T300	973.8	88.7	1.16
OxCr-T600	907.7	96.2	1.13

The recent researchers to understand the pool boiling CHF enhancement mechanism have focused on the capillary wicking mechanism. In this mechanism, the liquid inflow driven by the capillary pressure is sucked into the microlayer around dry spots and delays the formation of dry patches [1]. This was revealed by directly observing the dynamic behavior of dry spot growth under water boiling [3].

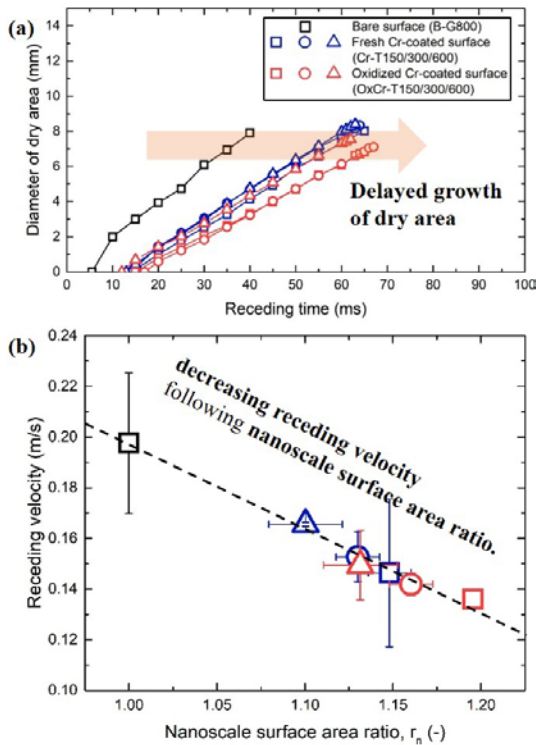


Fig. 4. Quantification of receding velocity: (a) trend of increasing diameter of dry area and (b) corresponding receding velocity compared with nanoscale surface area ratio.

To quantify the wicking characterization, we measured the increasing diameter of dry area following a receding time from the high speed images in Fig. 2(b) as shown in Fig. 4(a). Fig. 4(a) was sketched with a single data on each surfaces for a simplicity. Furthermore, we linearly-fitted a slope of increasing diameter of dry area with receding time, which was named by a receding velocity u_r . The average receding velocity of 3 repetitive experiments on each surfaces were confirmed with the range from 0.168 to 0.195 m/s. This results are quite similar with the nanostructure (0.19 m/s) in Son et al.[2]. Moreover, the receding velocity of fresh and oxidized Cr-coated surfaces was compared with a nanoscale surfaces area ratio r_n as shown in Fig. 4(b), which was measured by an atomic force microscopy (AFM) in the $5 \times 5 \mu\text{m}^2$ resolution as listed in Table II. This measurement noticed that the oxidized Cr-coated surfaces is 3-7 percent rougher than fresh Cr-coated surfaces and the decreasing trend following substrate temperature was confirmed before and after oxidation process. The receding velocities were escalated as lower surface area ratio (higher substrate temperature). The lower receding velocity implies that the capillary wicking potential of its surface is naturally high.

To verify the hydrodynamic similarity of a dry spot behavior between this air injection observation and a direct observation for water boiling, we calculated the dry area diameter same with the capillary length by using the measured receding velocity as shown in Eq. (2) [2].

$$D_{\text{dry}} = D_b - 2u_r t_r \quad (2)$$

Here, t_r is a receding time, which means an elapsed time that the dry spot grows up to be similar with the capillary length. As the calculated dry area diameter is larger, the amount of the wicked liquid in the microlayer under the nucleate bubble and the resultant enhancement in CHF is predicted to become smaller.

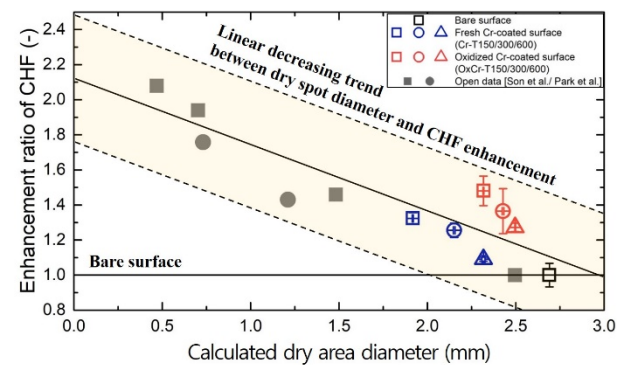


Fig. 5. Verification and comparison of calculated dry area diameter same with the capillary length with enhancement ratio of measured CHF.

Fig. 5 shows the comparison of resultant CHF enhancement ratio with the calculated dry area diameter on each surfaces. The enhancement in CHF showed a linearly good agreement with the decreasing dry area diameter. In addition, this results are consistent with the results of Son et al. [2] and Park et al. [4]. This trend

indicates that the expanding dry spot behavior of the receding situation by the air injection and the boiling situation is quite similar.

Following an above capillary wicking mechanism, the wicking-enhanced CHF $q''_{wicking}$ is directly proportional to a wicked liquid volume rate \dot{V}_w (Eq. (3)).

$$q''_{wicking} = \frac{\rho_l h_{fg}}{A_b} \dot{V}_w \propto \dot{V}_w = \dot{V}_w = \frac{1}{t_r} \int_{D_{dry}}^{D_b} \frac{\pi D}{R_{sm}} A_c dD \quad (3)$$

where ρ_l , h_{fg} , and A_b are a liquid density, a latent heat, and a bubble base area. By definition, the wicked liquid volume rate could be calculated as an integral form with variables such as the receding velocity t_r , the cross-sectional channel area A_c , the bubble base diameter ($D_b = \sqrt{\sigma_l/(\rho_l g)}$), and dry area diameter D_{dry} . The cross-sectional channel area could be calculated by multiplying the cross-sectional area of the microflow channel $A_{c,micro}$ with the nanoscale surface area ratio r_n as shown in Eq.(4). $A_{c,micro}$ is the product of an arithmetical mean height R_a and a mean width of the profile element R_{sm} [5], which were measured by AFM in the $30 \times 30 \mu\text{m}^2$ resolution as listed in Table II. The final form of the calculated wicked liquid volume rate substituted with above variables can be expressed as Eq. (5).

$$A_c = A_{c,micro} r_n = \frac{3}{2} R_a R_{sm} r_n \quad (4)$$

$$\dot{V}_w = \frac{3R_a r_n}{t_r} \left(\frac{\pi D_b^2}{4} \right) \left(1 - \left(1 - \frac{2u_r t_r}{D_b} \right)^2 \right) \quad (5)$$

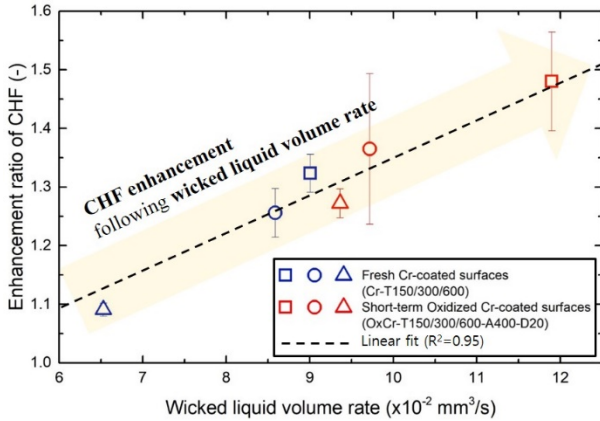


Fig. 6. Normalized CHF according to wicked liquid volume rate.

The calculated wicked liquid volume rates on the Cr-T150/300/600, and OxCr-T150/300/600 were 9.01, 8.59, 6.53, 11.90, 9.72, and $9.36 \times 10^{-2} \text{ mm}^3/\text{sec}$, respectively. Fig. 6 shows a strong linear relation between the calculated wicked liquid volume rate representing the capillary wicking potential and the amplified CHF on the fabricated surfaces. These results imply that the capillary wicking momentum and the resultant CHF is increased by the modified surface roughness because of the coating and the oxidation process.

4. Conclusion

Pool boiling experiments were conducted with Cr-coated surface by DC magnetron sputtering technique at substrate temperature of 150 °C, 300 °C, and 600 °C before and after oxidation at 400 °C during 20 days. In this study, the nanoscale roughness of all fabricated surfaces and the receding velocity of wicked liquid by injecting compressed air was measured to analyze CHF modification along with wicking characterizations of fresh and oxidized Cr-coated surfaces. It is confirmed that the receding velocity was decreased as following nanoscale roughness. Measured CHF enhancement was compared with the calculated dry area diameter for the verification of the experiment and shows the inversely linear relation. In addition, amplified CHF has a strong linear relation with the calculated wicked liquid volume rate. In conclusion, the CHF enhancement of fresh and oxidized Cr-coated surfaces could be increased by the capillary wicking effect which hinders the growth of dry area underneath the nucleate bubble. Importantly, the further CHF enhancement after oxidation process implies that the thermal margin of the coated cladding would not be threaten even if it is exposed under the normal operating condition in nuclear reactor.

Acknowledgement

This research was supported by the National Research Foundation of Korea (NRF) grant funded by the Korean government (MSIP: Ministry of Science, ICT and Future Planning) (No. NRF-2018M2A8A5025901)

REFERENCES

- [1] M. M. Rahman, E. Ölçeroglu, and M. McCarthy, Role of wickability on the critical heat flux of structured superhydrophilic surfaces, *Langmuir*, Vol.30(37), 2014, p.11225–11234.
- [2] H. H. Son, N. Kim, and S. J. Kim, Novel measurement of receding wicked liquid responsible for critical heat flux enhancement, *International Journal of Heat and Mass Transfer*, Vol.124, 2018, p.150–157.
- [3] D. I. Yu, H. J. Kwak, H. Noh, H. S. Park, K. Fezzaa, and M. H. Kim, Synchrotron x-ray imaging visualization study of capillary-induced flow and critical heat flux on surfaces with engineered micropillars, *Science Advances*, Vol.4(2), 2018, p.37–42.
- [4] Y. Park, H. Kim, J. Kim, and H. Kim, Measurement of liquid-vapor phase distribution on nano- and microstructured boiling surfaces, *International Journal of Multiphase Flow*, Vol.81, 2016, p.67-76.
- [5] H. H. Son, Y. S. Cho, and S. J. Kim, Experimental study of saturated pool boiling heat transfer with FeCrAl- and Cr-layered vertical tubes under atmospheric pressure, *International Journal of Heat and Mass Transfer*, Vol.128, 2019, p.418–430.